Surveys in Geophysics (2005) 26:675–700
DOI 10.1007/s10712-005-1830-3

MARINE CONTROLLED SOURCE ELECTROMAGNETICS: PRINCIPLES, METHODOLOGIES, FUTURE COMMERCIAL APPLICATIONS*

NIGEL EDWARDS
Department of Physics, University of Toronto, Toronto, Ontario, Canada M5S 1A7
E-mail: edwards@core.physics.utoronto.ca

(Received 8 April 2005; accepted 25 May 2005)

Abstract. The exploration community, from the earth scientist to the investment manager, has surely recognized the recent surge of interest in the use of controlled source electromagnetics for offshore hydrocarbon detection and assessment. The targets, petroleum, natural gas and gas hydrate, are resistive zones in an otherwise conductive background. I trace the academic and commercial development of marine methods from basic theory through experimental design to the few published relevant exploration case histories.

Keywords: electromagnetics, exploration, gas hydrate, investment, marine, petroleum

1. Academic and Commercial

In their review of marine electromagnetic methods written almost 20 years ago, Chave et al. (1986) comment that while electromagnetic exploration of the solid earth was quite active in academic circles since 1970, the adoption of the technology by exploration companies was surprisingly slow even though some majors including Exxon were undertaking in-house research (Len Srnka, personal communication). Meanwhile, the search for hydrocarbons was progressing from the continents offshore, into progressively deeper water, making the continental shelves a focus for seismic activity. The success of the seismic approach alone was evident by the level of offshore drilling activity and the subsequent production of oil. However, there are marine geological terranes in which the interpretation of seismic data is difficult, including regions dominated by scattering or high reflectivity, such as those found over carbonate reefs, areas of volcanics and submarine permafrost. Complementary geophysical techniques are required to study these regions.

*Invited review paper presented at the 17th Electromagnetic Induction Workshop. Hyderabad, India, 18–23 October, 2004.

Electromagnetics was at first not high on the list of alternatives. There was a pervasive belief that the high electrical conductivity of sea water precluded the application of electromagnetic systems for exploration. Academics had put forward methods specifically designed for the marine environment many differing in concept, instrumentation and methodology from their standard terrestrial cousins but the interest remained minimal for more than two decades.

The tide turned when a few surveys commissioned from universities proved very successful and in less than 5 years, exploration managers and investors have become aware of the importance of the recent developments. For example, Morgan Stanley, a well-known member of the New York Stock Exchange and an Investment Manager, reported in August 2004 on their assessment of the prospects of two companies – OHM, based in Aberdeen, Scotland, and partially owned by Southampton University, UK, and EMGS, a spin-off company of Statoil, based in Norway, who learned their skills from Southampton and the Scripps Institution of Oceanography, San Diego, USA. Morgan Stanley make passing reference to some of the many patents that have been taken out in the last 2 or 3 years, (Eidesmo et al., 2003; Ellingsrud et al., 2003; Srnka, 2003). In their view the implications of controlled source electromagnetic imaging (CSEMI) on offshore drilling, service, and field development activity will be one of the most frequently discussed topics in the oil service industry over the next 12 months. They see a growth in annual revenues from a mere $30 million to $600–900 million in less than 5 years – one quarter of the current spending on offshore seismic and compare the technological revolution with the growth of 3D seismic in the early 1990s.

One has to be careful reading such optimistic forecasts based on perceived scientific activity and patents as they are not the refereed publications that we as a community respect. Morgan Stanley may even represent the companies involved. Nevertheless, the buzz in the industry is quite real and the science on which the methods are based was published by a small number of academic groups in well respected journals.

In my brief review, I will try to trace the academic advances relevant to hydrocarbon exploration and point the reader at some subsequent commercial case histories.

2. Electrical Conductivity

The electrical conductivity of petroleum, free gas or hydrate bearing sediments is based on the concept of an increased resistivity in hydrocarbon-rich zones. We can use Archies law (Archie, 1942) to relate measured bulk resistivities to porosity estimates for a simple two-phase system that consists of the resistive grain matrix and the conductive pore fluid. In a general form, it is

$$\rho_f = a\rho_w\phi^{-m},$$

where ρ_f is the measured formation resistivity, ρ_w is the resistivity of seawater, ϕ is the sediment porosity, a is a constant and m the cementation factor. The latter two parameters can be derived from laboratory measurements and vary between $0.5 < a < 2.5$ and $1.5 < m < 3$. To calculate the resistivity of a similar rock containing in addition resistive petroleum, gas or gas hydrate, we have to modify the above formula. A modified formula is typically

$$\rho_f = a\rho_w\phi^{-m}S^{-n}. \tag{2}$$

The parameter S is now the pore water saturation factor, n the saturation coefficient and $S_h = (1-S)$ is the hydrocarbon saturation.

3. DC Methods – MOSES

Conventional static low frequency current (DC) methods are not particularly sensitive to resistive zones in the sea floor. A current from a dipole source on the sea floor flows mainly in the sea water and potentials measured at a receiver dipole are controlled by the conductivity of the sea water. MOSES, an acronym which stands for Magnetometric Off-Shore Electrical Sounding, based on the Magnetometric Resistivity (MMR) method offered an alternative (Edwards et al., 1981). The transmitter is a vertical long wire extending from the sea surface to just above the sea floor, as shown in Figure 1 and can be moved by the ship laterally. A commutated current is fed through the wire to two electrodes: one near the sea surface, the other on the sea floor. The return current is through the sea water and the subjacent crust. The receiver consists of two orthogonal horizontal magnetic field detectors located stationary on the sea floor. The measured data are the two horizontal components of the magnetic field as a function of frequency and transmitter–receiver separation. Accurate estimates of sea floor conductivity are possible with this configuration because the horizontal magnetic field is proportional to the current which enters the crustal material. Ampere's circuital law is applied to a horizontal circuit on the sea floor, centered at the base of the current bipole. The total current flow for a uniform sea layer above a uniform layered earth has axial symmetry about a vertical axis defined by the bipole. The azimuthal magnetic field is constant in magnitude around the Ampere circuit and is due only to the current which crosses the plane of the circuit, the current which enters the sea floor). This current may be shown to be proportional to the ratio of the sediment conductivity to that of seawater. Consequently, the associated magnetic field is a direct measure of the basement conductivity.

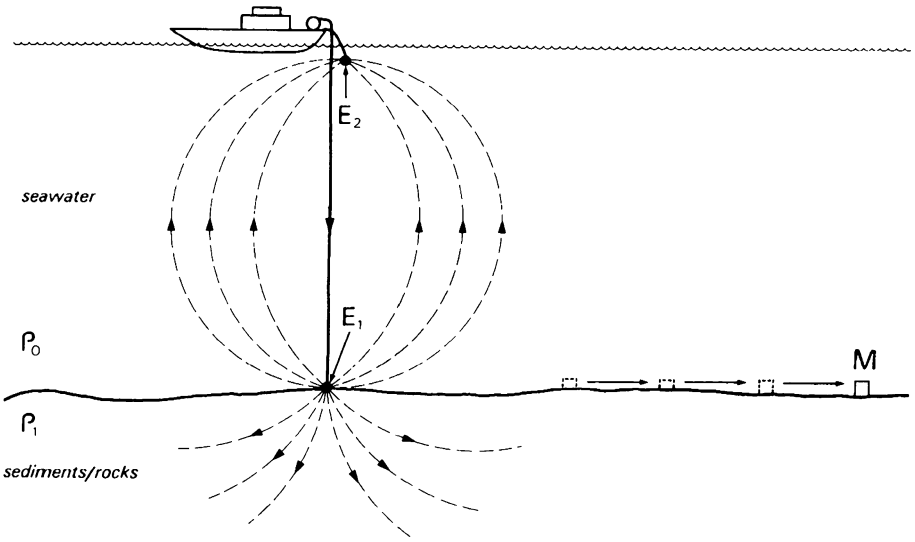

Figure 1. Schematic illustrating the principle of the MOSES method. The current flow is axisymmetric about the bipole source. The relatively small amount of current entering the resistive crust is proportional to the ratio of the crustal to seawater conductivities. By Ampere's circuital theorem, only this current contributes to the azimuthal magnetic field measured at a point on the seafloor.

A relevant successful sea test of a MOSES system is described by Edwards et al. (1985). The test area, Bute Inlet, is located approximately 200 km NW of Vancouver, British Columbia, Canada. The inlet is more than 50 km long and averages 3 km in width. It is a vee-shaped valley containing seawater about 650 m deep, overlying sediment estimated to be 600 m thick by extrapolating the shape of the adjacent topography downwards beneath the sea. The apparent resistivities and the associated errors shown as crosses in Figure 2 were computed from the field data taken along an axial profile down the inlet. The range of separation of the transmitter and receiver is 150–2000 m. The averaging recording time at each station was 1 h. The operating frequency was 0.125 Hz, which is just low enough to allow the effects of EM induction to be neglected and the static approximation to be valid. Errors in apparent resistivity at short separations are principally due to errors in position, whereas those at large separation are due to errors in magnetic component estimation. The local geology beneath the sea can be modelled by one layer over a half space. The layer represents the conductive sediment and the half space the relatively resistive basement rock. The best fitting model is inset into Figure 2 and has a ratio between the half space and the sedimentary layer of 51. The corresponding type curve is shown as a very heavy line. The data do not fit lower ratio curves. The estimates of the sediment thickness and resistivity determined by the technique are reasonable. The sediment

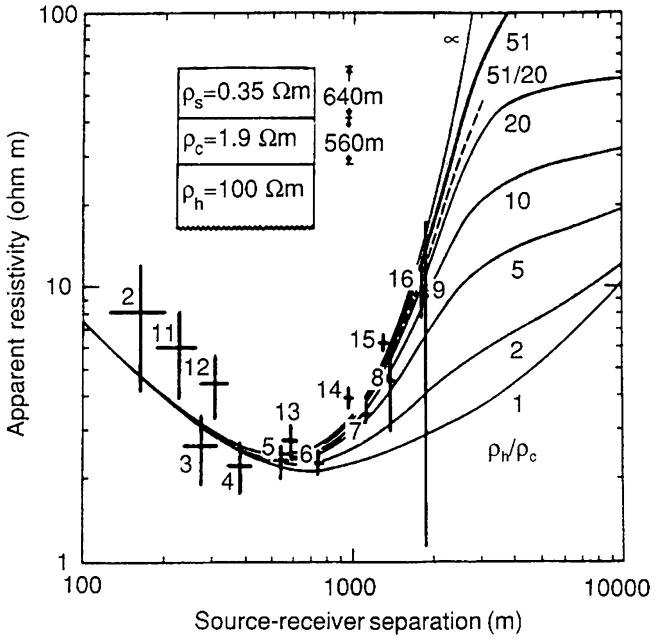

Figure 2. Numbered crosses are MMR data shown as apparent resistivities as a function of transmitter–receiver separation for the Bute Inlet. The curves are the model of a layer over a more resistive half space beneath the sea shown in the inset. The best fitting model has a ratio of 51 between half space and sedimentary layer resistivities.

resistivity of 1.9 Ωm corresponds to a porosity of about 42%, which is in the range of that measured on local core samples. The thickness of the sediments, estimated at 560 m, is less than the upper estimate of 600 m obtained by extrapolating the shape of the adjacent topography downwards beneath the sea. It is also a value in good agreement with that obtained by reflection seismology. The interpreted range of basement resistivity does include that of typical crystalline rock. The MOSES method has been used by my group in Cascadia (Nobes et al., 1986), the Beaufort Sea (Edwards et al., 1988), by colleagues in Japan and at Woods Hole, USA (Evans et al., 1998). It has become a popular exploration method for detecting resistive and conductive zones in the sea floor and attracted the attention of 3D numerical modelers (Chen et al., 2002). The code developed is an example of the modification of pre-existing software for marine studies.

4. AC Methods

An AC-controlled source system consists of a transmitter capable of generating an electromagnetic disturbance in the ground and one or more receivers

which detect the disturbance at some later time as it passes nearby. Similar to land-based systems commonly used for mineral prospection, the transmitter and the receiver may be electric and/or magnetic dipoles. Usually, for marine exploration, both the transmitter and the receivers are near or on the sea floor, as shown in Figure 3. Further, the system response can be described in frequency domain, time domain and transient domain. I place transient systems in a separate category as for such systems the received signal is measured after the transmitted signal has been turned-off to remove the primary signal that propagates through the 'air' and improve the relative strength of the secondary signal. The frequency and time domain systems use a continuous waveform. On the sea floor, there is no particular advantage to the transient system as there is no primary signal. I prefer describing the physics in time domain, but the time and frequency domains are essentially equivalent. In particular, delays in time domain are related to phase changes in frequency domain.

4.1. The response of a layered earth

I have found a study of the nature of the response of a layered earth to a time domain controlled source system to be a useful learning exercise, as some of

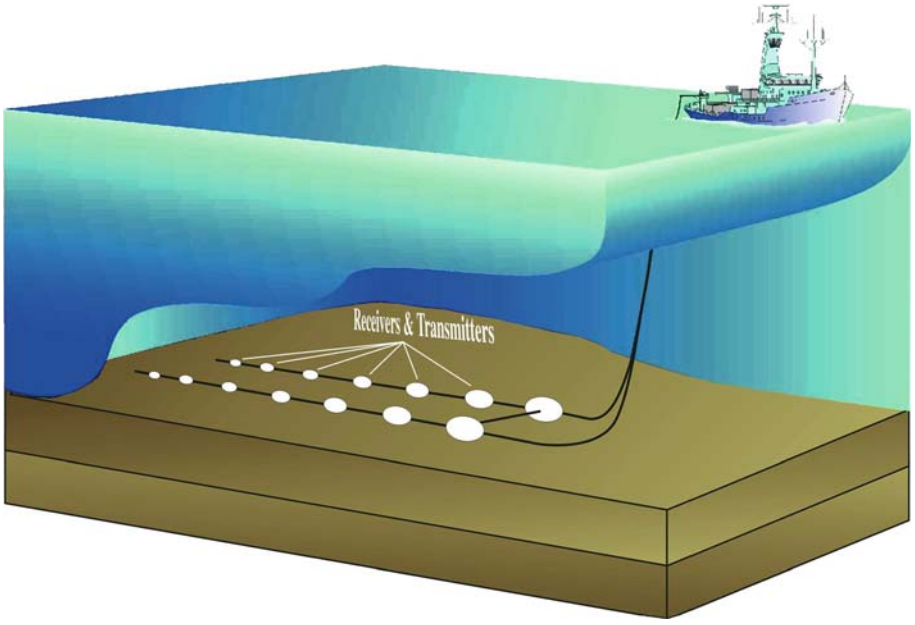

Figure 3. Possible design of a towed electric seafloor array. Transmitter and receiver electrodes are interchangeable and pairs can be connected to generate many dipole–dipole configurations.

the physics is counter intuitive. Disturbances from the transmitter diffuse through the seawater and the sea floor and are seen at the receiver as at least two distinct arrivals separated in time depending on the conductivity contrast between sea water and subjacent crust. If the layered sea floor increases in resistivity with depth, then disturbances propagate laterally more rapidly at depth than immediately beneath the sea floor. The received signal viewed at different ranges in logarithmic time has many of the characteristics of refraction seismic, even though the process is diffusive, and can be processed using seismic methods. We use two basic configurations for marine exploration: The horizontal coaxial magnetic dipole–dipole and the horizontal electric dipole–dipole. The latter system can be arranged in broadside and in in-line geometries. The two geometries yield different information (Yu and Edwards, 1991; Yu et al., 1997). For example, the in-line electric dipole–dipole is sensitive to the vertical resistivity whereas its broadside cousin is sensitive to the horizontal resistivity perpendicular to the line joining the dipoles. The electromagnetic fields impressed in the crust by both the horizontal magnetic dipole and the horizontal electric dipole have two polarizations. The polarizations are characterized by the absence of a vertical magnetic field and a vertical electric field respectively. They average the resistivity in two different ways. If these averages are different, then the medium appears to be only laterally isotropic. Data collected over layered Earth structures must be interpreted using software including anisotropy either as multiple fine isotropic layers or, better, as a few anisotropic layers.

4.2. Theory

My review does not contain detailed mathematical derivations as these are already published in the academic literature. I offer a summary of the layered earth responses for the electric dipole–dipole system for the in-line and broadside configurations, following Chave and Cox (1982), Edwards and Chave (1986), and Cheesman et al. (1987). I assume the sea water has a finite thickness d_0 and an electrical conductivity σ_0. The permittivity of the air is ϵ. The subjacent crust has N layers with thicknesses d_1, d_2, ..., $d_{N\text{-}1}$ and conductivities σ_1, σ_2 ,..., σ_N, respectively. I assume a current I is switched on at time $t=0$ and held constant in a transmitting electric dipole of length Δl. The expression for the Laplace transform of the step-on transient electric field at the sea floor for the in-line electric dipole–dipole geometry, dipole separation ρ, is given in terms of s, the Laplace variable. It is

$$\frac{I\Delta l}{2\pi s}[F(s)+G(s)], \tag{3}$$

where F and G are the Hankel transforms

$$F(s) = -\int_0^\infty \frac{Y_0 Y_1}{Y_0 + Y_1} \lambda J_1'(\lambda\rho) d\lambda,$$

$$G(s) = -(s/\rho) \int_0^\infty \frac{Q_0 Q_1}{Q_0 + Q_1} J_1(\lambda\rho) d\lambda, \tag{5}$$

and the included Laplace transform of the source dipole moment is $I\,\Delta l/s$.

If the magnetic effects of displacement currents in the earth are neglected, then the parameters Y_0 and Q_0 are given for the sea layer as

$$Y_0 = \frac{\theta_0}{\sigma_0} \left[\frac{\sigma_0 u_a + s\epsilon\theta_0 \tanh(\theta_0 d_0)}{s\epsilon\theta_0 + \sigma_0 u_a \tanh(\theta_0 d_0)} \right] \tag{6}$$

and

$$Q_0 = \frac{\mu_0}{\theta_0} \left[\frac{\theta_0 + u_a \tanh(\theta_0 d_0)}{u_a + \theta_0 \tanh(\theta_0 d_0)} \right], \tag{7}$$

where the electromagnetic wavenumbers in the ground and in the air are given by $\theta_0^2 = \lambda^2 + s\mu\sigma_0$ and $u_a^2 = \lambda^2 + s^2\mu\epsilon$.

The parameters Q_1 and Y_1 are evaluated through the down-counting recursion relationships

$$Y_i = \frac{\theta_i}{\sigma_i} \left[\frac{\sigma_i Y_{i+1} + \theta_i \tanh(\theta_i d_i)}{\theta_i + \sigma_i Y_{i+1} \tanh(\theta_i d_i)} \right], \tag{8}$$

and

$$Q_i = \frac{\mu_0}{\theta_i} \left[\frac{\theta_i Q_{i+1} + \mu_0 \tanh(\theta_i d_i)}{\mu_0 + \theta_i Q_{i+1} \tanh(\theta_i d_i)} \right], \tag{9}$$

where the starting values are $Y_N = \theta_N/\sigma_N$ and $Q_N = \mu_0/\theta_N$ respectively. The wavenumbers θ_i are defined by $\theta_i^2 = \lambda^2 + s\mu\sigma_i$.

The Y and Q functions denote the polarizations characterized by the absence of a vertical magnetic field and a vertical electric field, respectively. The Y function yields the DC 'resistivity' response at late time (Edwards, 1997).

The corresponding form for the broadside electric dipole–dipole geometry is as given in expression (3) but with alternative definitions for F and G, namely

$$F(s) = (1/\rho) \int_0^\infty \frac{Y_0 Y_1}{Y_0 + Y_1} J_1(\lambda\rho) d\lambda, \tag{10}$$

and

$$G(s) = s \int_0^\infty \frac{Q_0 Q_1}{Q_0 + Q_1} \lambda J_1'(\lambda\rho) d\lambda. \tag{11}$$

The methods for inverting the Hankel and Laplace transforms are fully described in the theoretical papers listed above. All other geometries are a linear combination of the in-line and broadside responses.

The frequency domain response of the dipole may be obtained by multiplying the step-on response by s and then replacing s by $i\omega$ where ω is the angular frequency of the harmonic current. The inverse Hankel transform becomes a complex function having a phase and an amplitude.

I have extended the codes to include the effects of anisotropy caused by interbedding. The coefficient of anisotropy k is defined by $k = \sqrt{\sigma_h/\sigma_v}$, where σ_h and σ_v are the tangential and normal conductivities in any given layer. The coefficient cannot be smaller than unity. I modify the form of θ only in expression (8) to $\theta^2 = k^2\lambda^2 + s\mu\sigma$. In both expressions (8) and (9), I replace σ_v by σ_h where ever it occurs.

4.3. Response curves

The step-on response of a double half space to the in-line electric dipole–dipole system is shown in Figure 4. The sea water is assigned a conductivity of 3 S/m while the subjacent crust has conductivities of 3, 1, 0.1 and 0.3 S/m respectively. The vertical axis has been scaled to yield the DC apparent resistivity at late time. The horizontal axis is in logarithmic time for a transmitter–receiver separation ρ of 260 m. (Absolute time may be estimated for any system given a conductivity σ and a value for ρ as $\mu_0\sigma\rho^2/c$, where c is a constant with a value of about 5. Progress of disturbances through several zones of differing conductivity may be obtained by summing such estimators).

The curves have three characteristics from which the conductivity of the crust may be obtained. There is late-time variation in amplitude, (Label 1), which is less sensitive with increasing conductivity contrast. There is an early time change in amplitude which depends on the sea floor conductivity, (Label 2). The location in time of this initial change is a strong function of sea floor conductivity (Label 3). My group uses this effect to determine apparent resistivity from time domain curves. The same information may be gleaned from amplitude and phase curves in the frequency domain.

4.4. Electromagnetic refraction?

I next display the diffusion of current from a 2D electric dipole at the junction of two half spaces representing sea water and the subjacent crust (Edwards, 1988). The diffusion is plotted as a series of contour maps for increasing time steps, as shown in Figure 5a–f. The magnetic field is out of the slide, the electric field is in the plane. The model is 500 m square and the

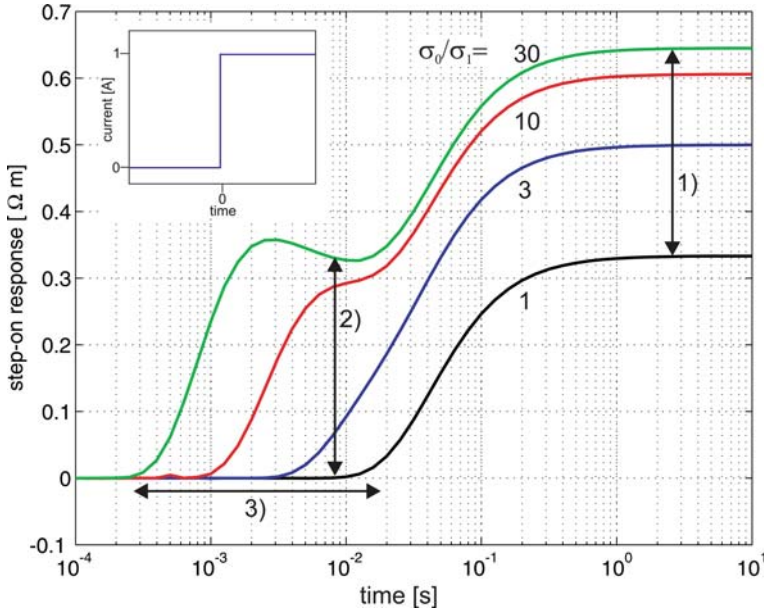

Figure 4. Normalized step-on responses calculated on the interface between two half spaces to the in-line electric dipole–dipole system. The conductivity of the upper half space is 3 S/m, for the lower half space conductivities of 0.3, 0.1, 1, and 3 S/m have been assigned. The separation between transmitter and receiver is 260 m. For a conductivity contrast between sea water and subjacent crust larger than 10 the arrival through the signal through the sea water at later times can be clearly separated from the earlier arrival through the crust. In addition, three different effects are noticeable: (1) Amplitude variations at late times depend on the conductivity contrast, but are mainly due to current flow through the sea water; (2) amplitude variations at earlier times depend on the sea floor conductivity; (3) the location in time to the initial change is a function of the sea floor conductivity.

sea water and crust have conductivities of 3 S/m and 0.5 S/m. The contours, originally shown in Edwards (1988), are current streamlines and the shading is proportional to the size of the electric field.

I often refer to the process as electromagnetic refraction, even though it is diffusive, because of the similarity of the lateral movement of the current flow pattern and the seismic head 'wave'. Consider the direction of Poyntings vector $\vec{P} \sim \vec{E} \times \vec{B}$. Clearly, the first arrival at a receiver dipole is a disturbance that has propagated through the more resistive zone, the crust. In the progress of the diffusion energy migrates upwards from the lower medium through the sea floor. At later times the signal that propagates through the sea water arrives and at the static limit (DC) symmetry is reached about the surface. The maps are consistent with the type curves presented in Figure 4.

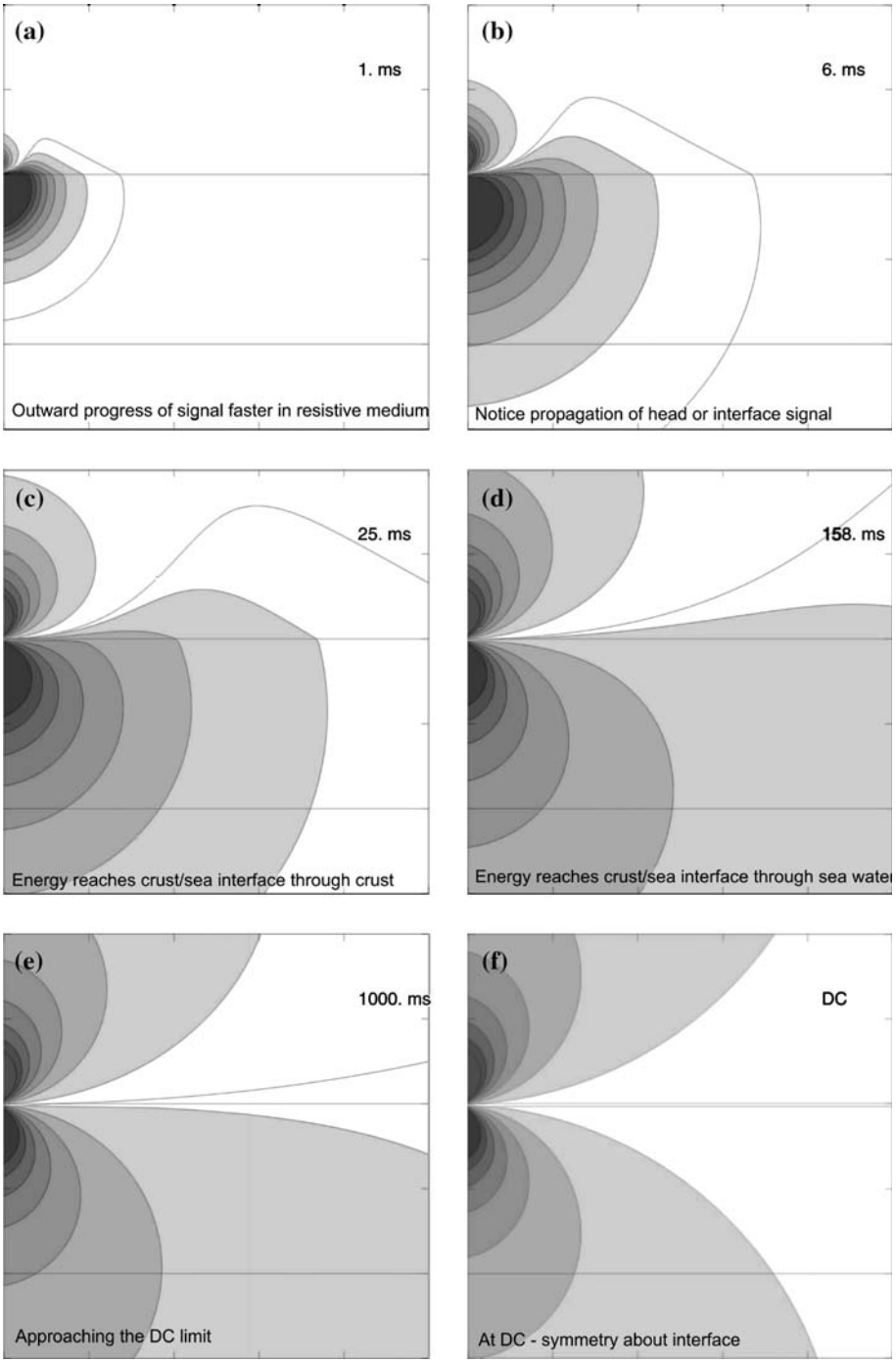

Figure 5. (a)–(f) Contour maps showing the diffusion proceeding with time of a current from a 2-D electric dipole at the interface of two half spaces representing sea water (3 S/m) and subjacent crust (0.5 S/m). The model is 500 m square. Contours are current stream lines of the electric field and the shading is proportional to the size of the field.

4.5. Seismic style displays

An impulse response may be obtained as the derivative with respect to logarithmic time of the step-on response. In the displays that follow, I have plotted the normalized impulse response as a function of logarithmic time and logarithmic transmitter–receiver separation. The amplitude scaling, which varies from figure to figure, yields the same curve at every offset for a simple double half space. The curve just moves to later time as the separation increases. The in-line electric dipole–dipole response has two peaks in the double half space impulse response corresponding to energy that has propagated through the sea and the crust respectively. The crustal peak is always at earlier time. Its broadside cousin also has two features but of different sign. The crustal peak is positive whereas the sea water trough at later time is negative.

4.5.1. *The air wave*

Of particular concern to companies who explore in shallow waters such as the shelf seas is the so called air wave. Some portion of the electromagnetic energy travels upwards to the sea surface, through the air to the vicinity of the receiver and then downwards to the receiver on the sea floor. The up-over-down path can in some instances be faster than any direct path through the sea water or the subjacent crust. Compare the two models shown in Figure 6a, b and the stacked impulse response of these models shown in Figure 6c–f, for the in-line and broadside geometries. The sea layer in the first model is infinitely thick while that in the second has a finite thickness of 200 m. As the transmitter–receiver separation increases, the air wave which initially appears at later time appears to move to relatively earlier times and at large separations contaminates the disturbance travelling through the crust. From a practical point of view, the air wave signature is easily removed in the inversion of data provided sufficient dynamic range in the receiver electronics is available to record it properly.

4.5.2. *The Resistive Zone at Depth*

In the second example, I show the responses of a double half space model modified by the inclusion of a rapid increase in resistivity at a depth of 200 m, as shown in Figure 7b and compare them with the base response of the half space model. The stacked impulse responses for the in line and broadside geometries are shown in Figure 7c–f. Notice the distinct refraction visible in the early time crustal response when the electromagnetic disturbance sees the resistive buried zone. The location of the refraction in space and its slope on the log time vs log separation diagram may be used to infer the depth to and conductivity of the resistive zone.

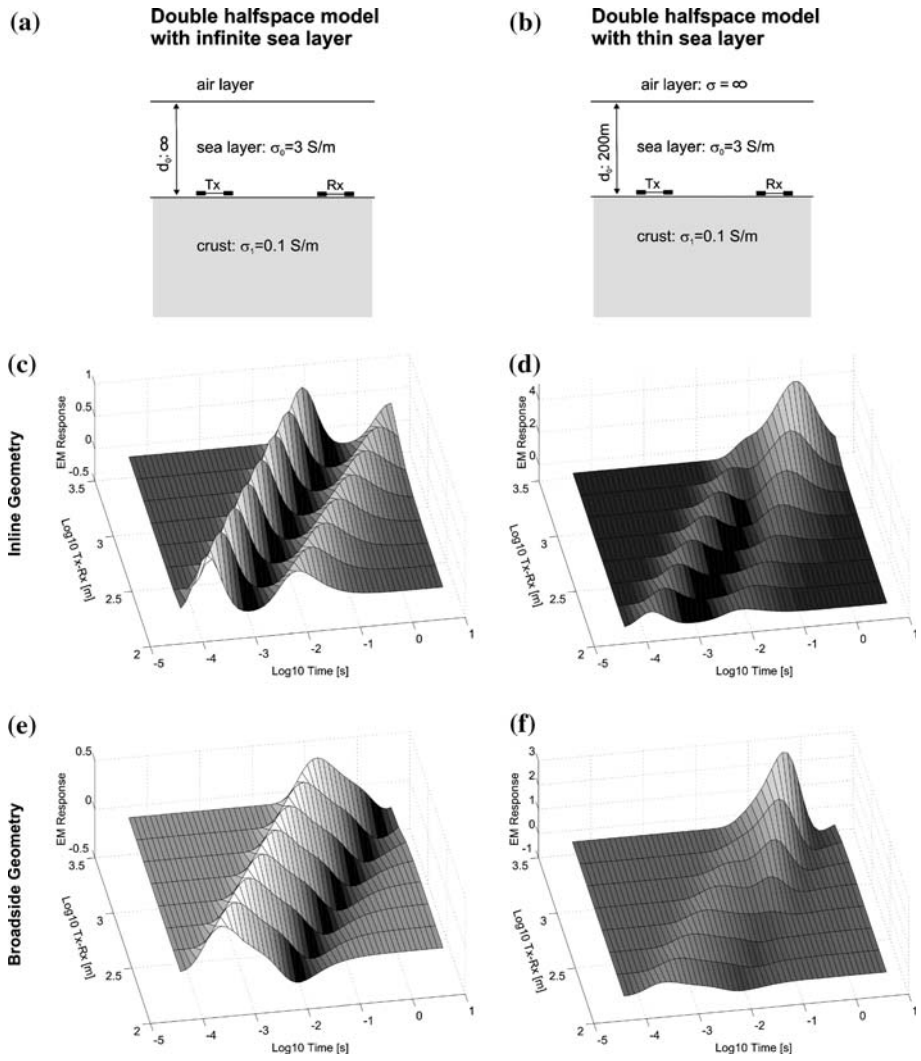

Figure 6. *The airwave*. The normalized impulse responses of the models in (a) and (b) to an electric dipole–dipole system on the seafloor are shown as functions of logarithmic time and transmitter receiver separation. Panels (c) and (d) refer to inline and panels (e) and (f) to broadside geometries.

5. Case Histories

5.1. The Troll gas field

The description of an electric dipole–dipole survey over the Troll gas field is found in Amundsen et al. (2004). The Troll field, WNW of Bergen, is the largest gas discovery on the Norwegian shelf. Water depth varies from 300 to 360 m. The overburden is between 1100 and 1200 m thick. The apparatus

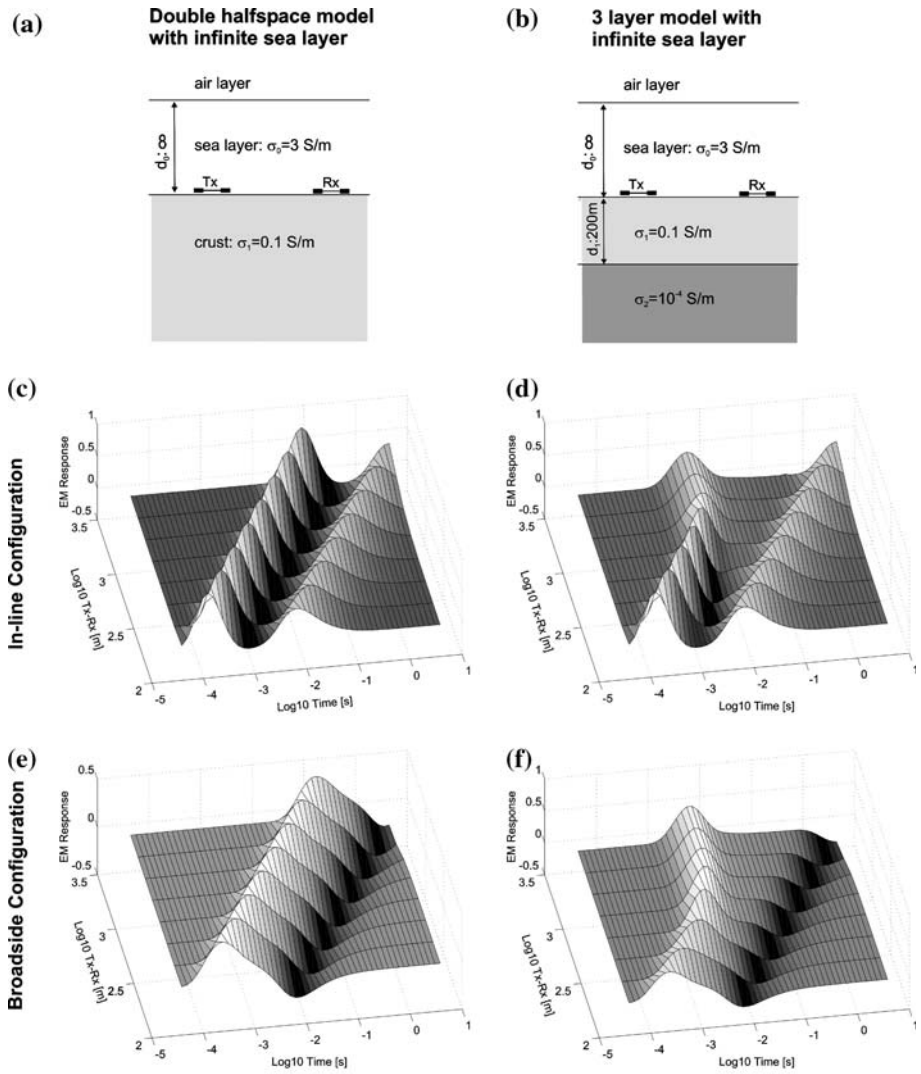

Figure 7. The resistive zone at depth. The normalized impulse responses of the models in (a) and (b) to an electric dipole–dipole system on the seafloor are shown as functions of logarithmic time and transmitter receiver separation. Panels (c) and (d) refer to inline and panels (e) and (f) to broadside geometries.

and methodology are similar to those described by Webb et al. (1985), Evans et al. (1994) and Sinha et al. (1997). A total of 24 electric field two-component receivers were dropped from a ship along a profile across the entire field and located by ultra short baseline (USBL) acoustics, as shown in Figure 8a. A transmitter dipole 230 m long was towed behind a ship just off the sea floor

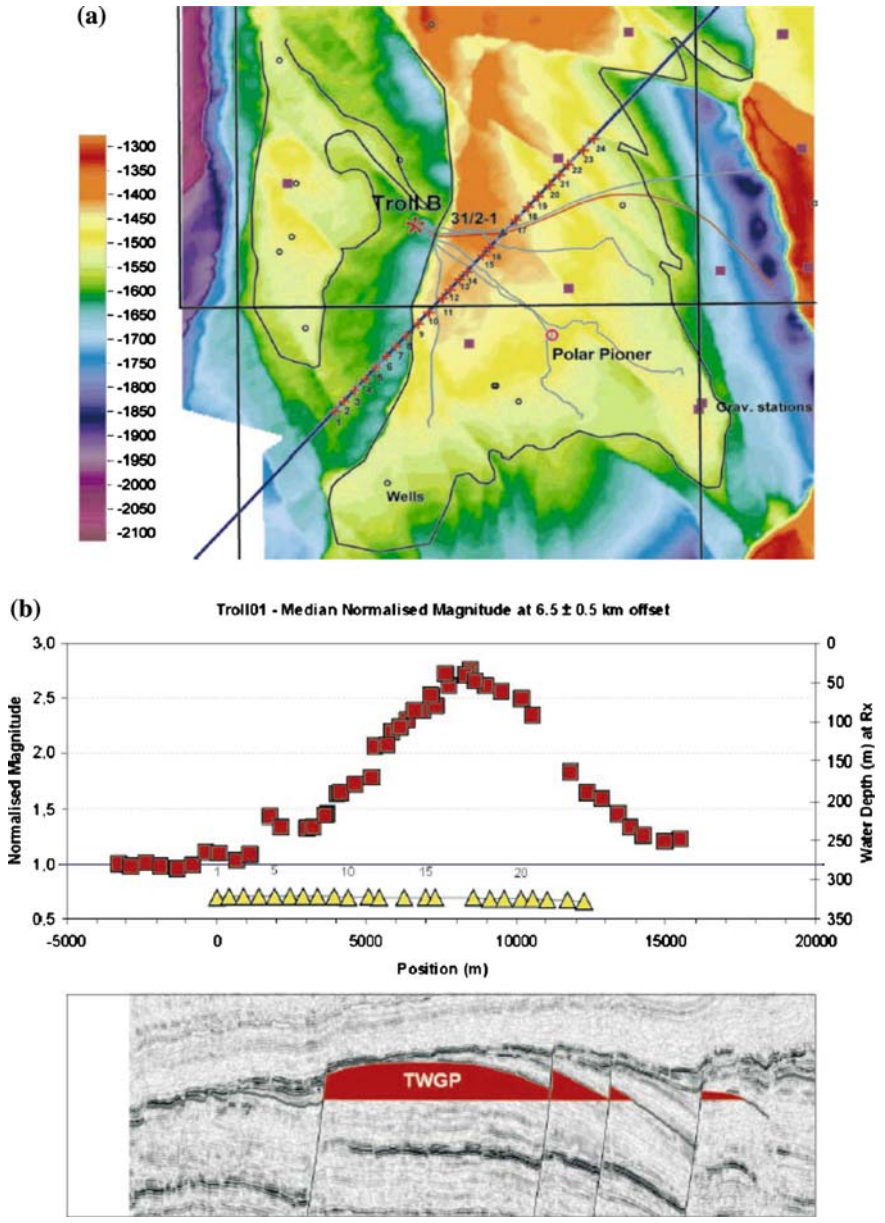

Figure 8. (a) Layout of receivers and towline on Troll Western Gas Province (TWGP). The reservoir is located in the jurassic Sognetfjord and Fensfjord formation. The top of the Sognetfjord formation is shown in the map. Positions of platform, drilling rigs, pipelines, gravity stations and exploration wells are also shown. (b) Normalized magnitude versus offset responses at 6–7 km after median filtering, together with receiver positions and a simplified section across TWGP. Transmitting frequency was 0.25 Hz. Median normalized magnitudes are posted 3.25 km from receivers at common midpoint positions (Amundsen et al., 2004).

on a SW to NE track. It can transmit frequencies in the range of 0.05–10 Hz. High quality data to an offset of 6–8 km were obtained.

The data were processed to yield a normalized response at an offset of 6.5 km. The results superimposed on a simplified section of the field are shown in Figure 8b. The anomaly correlates with the inferred boundaries of the field and has a value of close to 300% above the background value of the central parts of the hydrocarbon-rich zone. The results are consistent with reservoir interval resistivities of 70 Ωm compared with normal sediment values of 0.5–2 Ωm.

5.2. Angola

The electromagnetic survey in Angola is described by Ellingsrud et al. (2002). The petroleum prospects offshore are in a deep Tertiary basin, a sequence of sands and shales 10–20 km thick. The area is characterized by allochthonous salt of Aptian age and deep water channel sands with petroleum potential. Well logs give resistivity values in petroleum reservoirs similar to those in the Troll field. Over the survey area, the water depth is typically 1200 m and the overburden sediment thickness 1100 m. A shallow salt structure occurs in the NE corner of the target area.

A total of 26 receivers were deployed over a 3-D area and 23 recovered. The transmitter frequency was typically 0.25 Hz and the current 300 A peak to peak. The transmitter was towed a total distance of 314 km along 17 lines.

The anomaly is displayed in Figure 9a, b as normalized field ratios for the radial and azimuthal fields. The outline of the known hydrocarbon reservoir is shown in white. The large anomaly in the NE is the salt deposit. It appears on both maps while the petroleum reservoir is evident mainly on the radial data.

5.3. Gas hydrates in Cascadia

A report of an EM survey for gas hydrate off the west coast of Vancouver Island, Canada is presented by Schwalenberg et al. (2005) using apparatus originally developed by Yuan and Edwards (2000). Natural gas hydrates are ice-like solids that occur worldwide in sea floor sediments along continental margins. They consist of gas molecules, mainly methane, contained in a cage-like clathrate structure of water molecules. They form under low temperature and high pressure conditions, typically in the uppermost few hundreds of metres of sediments in water depth exceeding about 500 m. The global abundance of methane frozen in hydrate exceeds the amount of all other known fossil hydrocarbon resources. Hydrate clearly has a huge potential as a future energy resource. A gas hydrate deposit can be generally identified in a seismic section by the occurrence of a bottom simulating reflector (BSR)

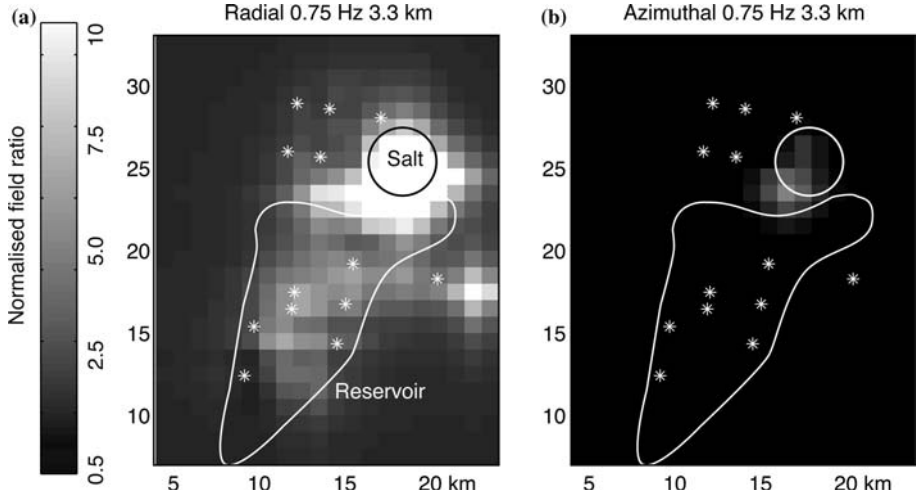

Figure 9. Results from a CSEM survey offshore Angola over a known oil reservoir. Normalized magnitude of 0.75 Hz electric fields at the sea floor for a range bin of 3000–6000 m is plotted as a function of midpoint across the survey area. Also shown for reference is the approximate outline of the known hydrocarbon reservoir and a salt structure (solid white lines). (a) shows predominantly radial fields (in-line configuration), (b) shows predominantly azimuthal field (broadside geometry). The large anomaly in the northeast is visible in both radial and azimuthal fields. The smaller anomalies which are confined to the radial data over the rest of the survey correspond to the known petroleum reservoir. Data to the south and northwest lack a significant radial response and show the limits on the lateral extend of the reservoir (Ellingsrud et al., 2002).

which is associated with the base of the hydrate stability field. The base is a transition zone between hydrate-bearing sediments above it and free gas and water below it. The location of the zone is temperature-controlled and depends on the ambient geothermal gradient. The target area is located on the accretionary prism of the Cascadia margin in close vicinity of ODP Site 889, as shown in Figure 10. Here, several seismic blank zones were observed over a vent field which covers an area of roughly 1×3 km. The largest, blank zone 1 is called the Bullseye vent and has a sea floor diameter of about 400 m.

The CSEM experiment was conducted in SW–NE direction, into the prevailing wind and current, along a profile intersecting the Bullseye and approaching the other vent sites, making measurements at 28 sites with an spacing between sites of 250 m. The sea floor array is towed in direct contact with the soft marine sediments, as sketched in Figure 11. At the forward end, a heavy weight (pig) is attached to keep the system in contact with the sea floor. It is followed by a transmitter dipole (TX) 124 m long and, in this experiment, just two receiver dipoles (RX1) and (RX2), each 15 m long located at distances r_1 and r_2 of 174 m and 292 m from the transmitter cable, respectively. Each receiver dipole consists of a pair of silver/silver chloride

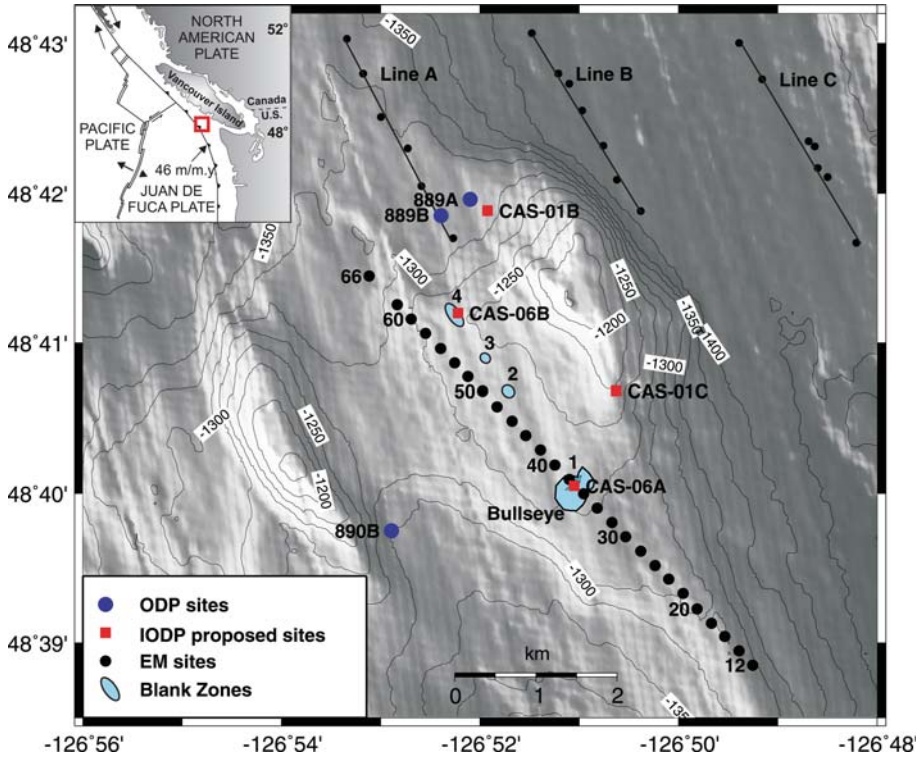

Figure 10. Bathymetry map of the target area on the Cascadia margin. The vent field is located on a bench between two topographic highs in vicinity of ODP sites 889/890. CSEM measurements were conducted along the profile crossing the Bullseye, the largest of four vent sites. Lines A, B, and C are EM profiles from a previous survey (Yuan and Edwards, 2000).

electrodes. It has its own amplifier, synchronous clock, processor and data storage. The sea floor system is attached to a coaxial cable which carries the transmitter current generated onboard the ship to the transmitter dipole. A photograph of shipboard operations is presented in Figure 12. The transmitter current voltage analogue is attached to similar electronics to those used by the receiver array so that phase differences between the various elements can be measured. While the system is operated in the time domain, using a square current waveform with a peak-to-peak amplitude of 20 A and a period of 6.6 s, the data analysis and inversion to a multi-layered model is completed in frequency domain using phase data only in the band from 0.5 to 100 Hz.

Simplified results for a half space model are plotted in Figure 13a for both receiver separations over a compatible seismic section, Figure 13b. Two pronounced resistivity anomalies are visible along the profile which are in striking agreement with the sea floor projections of the vent sites from the seismic section. The result is remarkable given the uncertainty of order 100 m

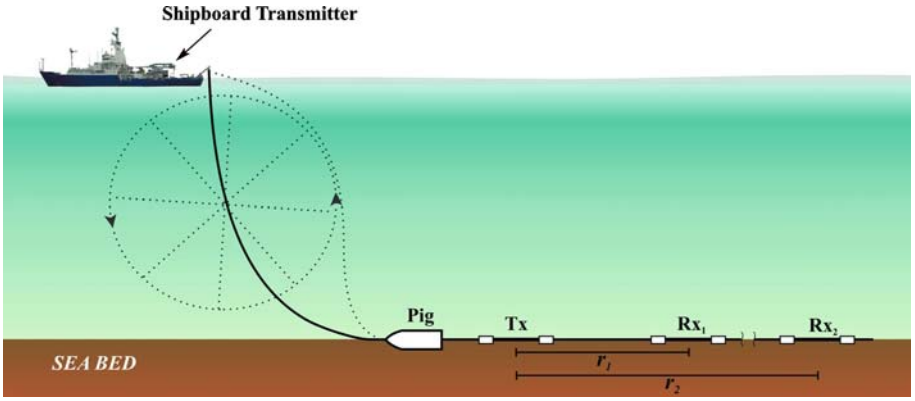

Figure 11. Geometry of the inline dipole–dipole configuration. A current signal is produced by an onboard transmitter and sent through the coaxial winch cable to the transmitter bipole on the seafloor. Two receiver dipoles at distances r_1 and r_2 record the signal after it passes through the seawater and the sediments. A heavy weight (pig) attached to the front of the system keeps the array on the seafloor while moving along the profile. Moving the ship and taking in the winch cable pulls the array forward and causes a vertical movement of the pig. Solid and dotted line present the winch cable in idle and moving state, respectively. The wheel represents the curve over which the marine cable appears to move while in motion.

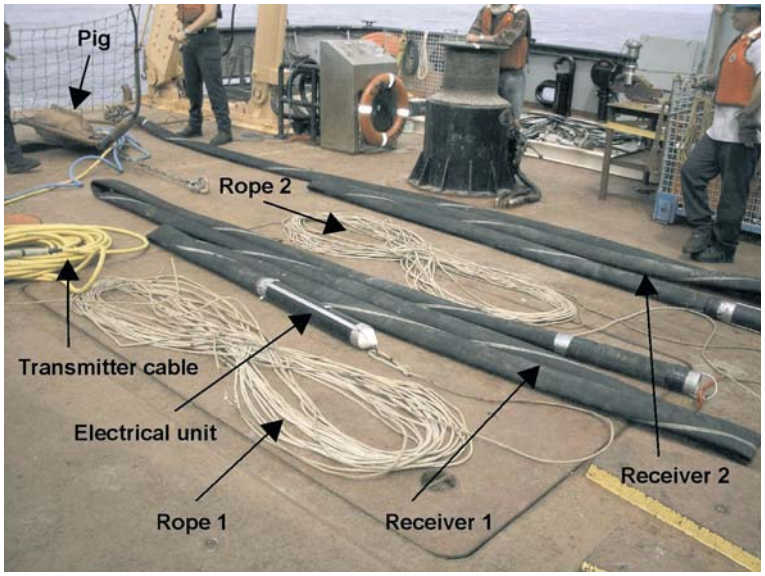

Figure 12. The University of Toronto electric dipole–dipole system aligned on the ship's deck before deployment. Receiver dipoles consist of pairs of silver–silver chloride electrodes mounted inside each end of a 15 m long rubber hose, suitable to be dragged along the sea floor. Receiver electronics consisting of a data logger, processor, synchronous clock, battery packs and amplifier inside a cylindrical pressure cage is attached to each receiver. Copper braid electrodes, 30 cm long, are attached to each end of the 124-m long mantled transmitter cable. Transmitter and both receivers are connected with Kevlar rope.

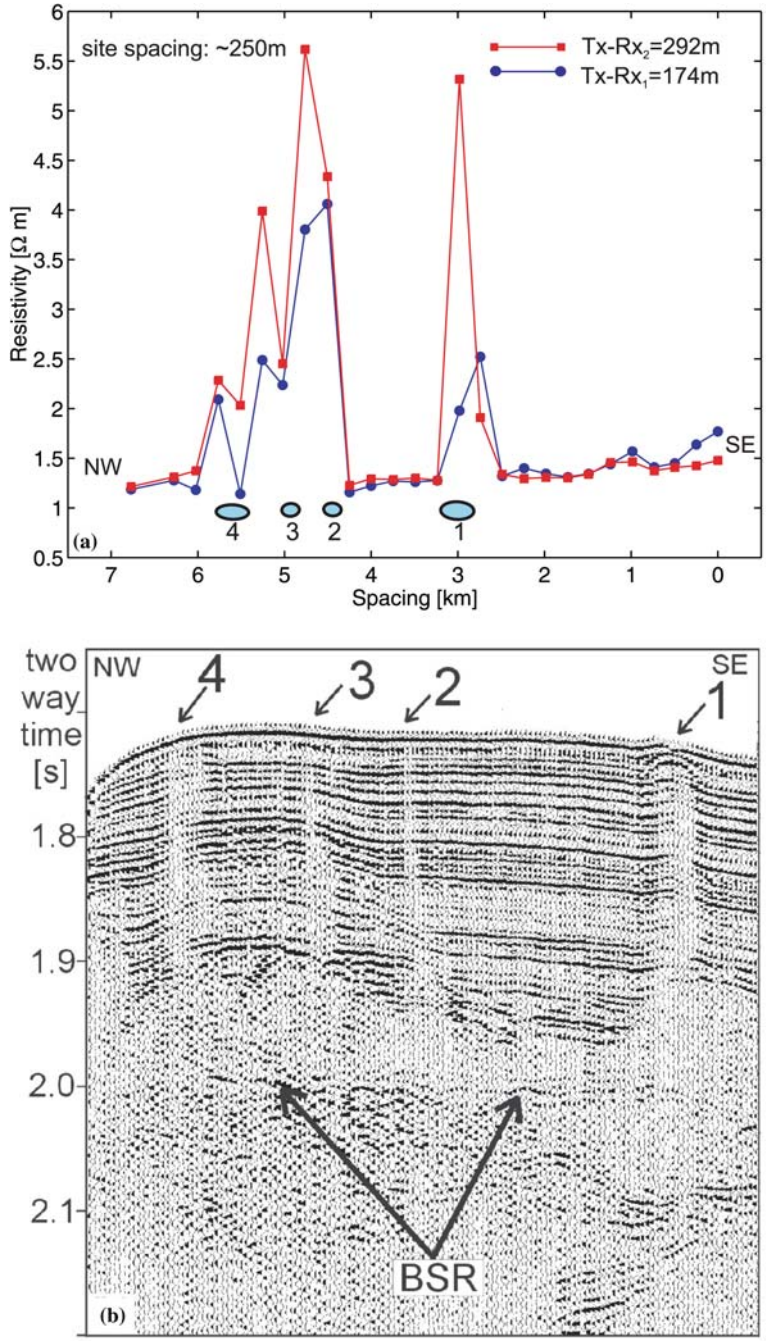

Figure 13. (a) Bulk resistivities derived from CSEM data show anomalous resistivities exceeding 5 Ωm over background resistivities between 1.1 and of 1.5 m. The anomalous areas coincide spatially with the surface expression of a series of seismic blank zones displayed in (b).

in the relocation of receiver positions from the GPS ship positions, water depth and cable length readings. The resistivity values within the anomalous zones are higher for the larger separation RX2 than those for RX1 and rise up locally to more than 5 m over the regional background, which lies between 1.1 Ωm and 1.5 Ωm . The gas hydrate concentrations derived from the resistivity profile, shown in Figure 14, over the vent sites exceeds 50% at maximum and about 25% on average of the available pore space.

The resolution of the CSEM method does not permit a detailed analysis of the distribution of the resistive elements within the blank zones but it does provide an integrated value. Assuming that the increase in resistivity is due to a higher hydrate concentration, the latter may be converted to total mass of hydrate and then to total available methane. A rough estimate can be made for the Bullseye vent assuming a cylindrical volume, with diameter and depth of 400 m and 200 m respectively. Twenty five percent of the available pore space corresponds to 3.8 million cubic metres. With a solid to gas ratio of hydrate of 1:164, the related methane gas volume at STP is 0.62 billion (US) cubic metres.

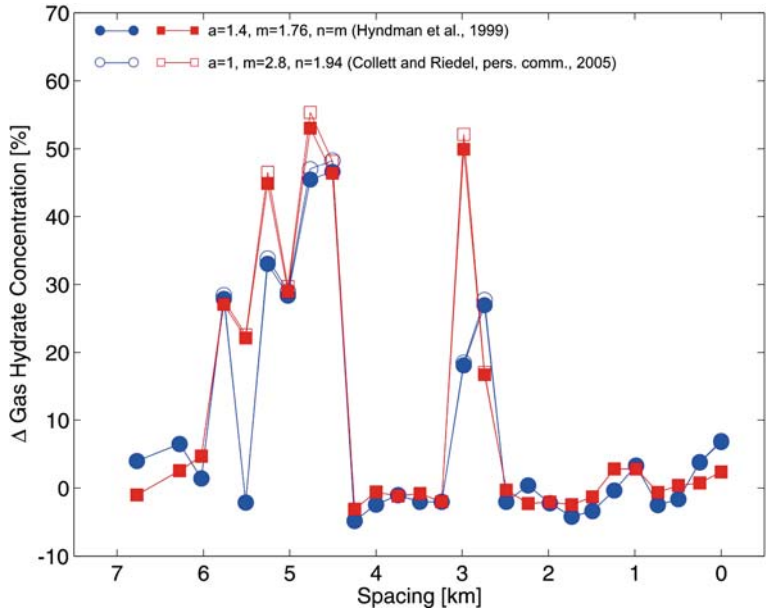

Figure 14. Gas hydrate concentrations derived from Archie's law using two different sets of Archie coefficients. The first set ($a = 1.4$, $m = 1.76$, $n = m$) is based on core data from ODP Leg 146 (Hyndman et al., 1999). A recent re-evaluation yielded a second set based on log data ($a = 1$, $m = 2.8$, $n = 1.94$) (Collett and Riedel, pers. comm., 2005). In this figure a regional gas hydrate concentration profile derived from the baseline resistivities in Figure 13a has been subtracted from the "total" hydrate concentrations. Thus, the profiles represent the additional amount of hydrate and are coincident for both sets of Archie coefficients.

5.4. Buried channels, New Jersey

Rob Evans group at the Woods Hole Institution of Oceanography and colleagues at the Geological Survey of Canada have built a small scale coaxial magnetic dipole–dipole system that is contracted for mainly shallow, geotechnical surveys. The system is a major improvement of systems described by Cheesman et al. (1990, 1991) and Webb and Edwards (1995). Among many other geological problems, they investigated the nature of the infill in a buried channel off-shore New Jersey (Evans et al. 2000). The buried channel represents one example of a feature in a shallow section that is an analogue to a feature seen in deeper oil bearing strata. The magnetic dipole system is dragged in contact with the sea floor. The three transmitter–receiver spacings are 4, 13 and 40 m. A picture of the system is shown in Figure 15.

Data collected in the frequency domain were processed to give an apparent porosity for each spacing. The maximum depth of investigation was about 20 m. Bounds on physical properties are greatly aided by complementary seismic survey. The latter identified the structure but alone offered no information on nature of the infill. The porosity traces and seismic section are shown in Figure 16a, b. Clearly, there is an excellent correlation between the buried channels visible on the seismic section and an increase of porosity. The channels seem to incise the regional seismic reflector.

Figure 15. Photo image of the magnetic dipole–dipole system. The system forms a 50 m long array on the seafloor and is dragged along the seafloor at speeds of 1–2 knots. It consists of a transmitter and three receivers at distances 4, 13, and 40 m from the transmitter, capable to investigate the shallow sediment structure to 20 m below the sea floor.

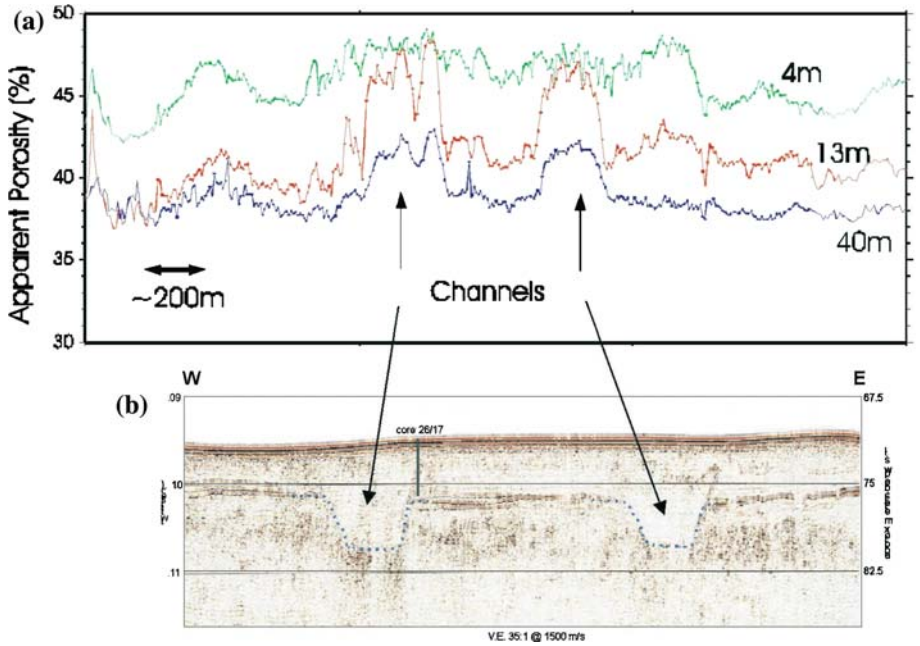

Figure 16. The magnetic dipole–dipole system has been used to find out the nature of the infill of buried paleo-channels on the New Jersey continental margin (Evans et al., 2000). (a) Apparent resistivities recorded at the three receivers have been converted to apparent porosities using Archie's law. A clear correlation between locally higher porosities and the seismic image of the paleo-channels in (b) is apparent.

6. Outlook

What does the future hold? McBarnet (2004) summarizes recent commercial activity and identifies the players involved. Both he and Steven Constable (SIO) credit the interest in the Statoil and the Exxon-Mobil surveys offshore Angola as kick starting all the major petroleum companies towards EM. Just how high the stakes are in the subject may be judged by the acquisition of EMGS by Statoil, of AGO EM, a spin-off of AOA (Arnold Orange) who cooperate with Scripps, by Schlumberger and by the valuation of OHM placed at over $100 million, with a current annual profit of about $1 million. Law suites between various parties are also being filed as well as a plethora of patents. The most recent player is from Edinburgh University (Ziolkowski and Hobbs, 2003) who name their nascent product MTEM – a purely time domain method.

In the next 5 years, we will see I believe a confluence of the shorter baseline towed transmitter and receiver methods and the towed transmitter, remote receiver technology, so that estimates of phase in frequency domain

may be made accurately. The bandwidth of the frequency domain systems will also be extended to approach that presently available in time domain. There is likely to be a confluence of seismic and electromagnetic thinking. EM data will be gathered in large arrays and optimal 3D methods to interpret array studies will be required. I know of some progress in 3D interpretation but I do not anticipate any immediate transfer to the public domain! I suspect modelers who can interpret 3D data are sitting on a very valuable commercial resource. There are however 2.5 D programmes available in both frequency and time domains using both finite element (Everett and Edwards, 1993) and finite difference algorithms (Unsworth et al., 1993).

I end on a very positive note. Undoubtedly, there will be positions available in the commercial environment for scientists skilled in marine EM. Come and join us!

Acknowledgements

I thank Katrin Schwalenberg very much for presenting the paper in India when I was advised, for health reasons, not to travel outside Canada. The research is supported by a grant from the Natural Sciences and Engineering Research Council of Canada.

References

Amundsen, H. E. F., Johansen, S., and Rosten, T.: 2004, 'A Sea Bed Logging (SBL) Calibration Survey over the Troll Gas Field', Paper presented at the 66th EAGE conference and exhibition, Paris, France, 7–10 June.

Archie, G. E.: 1942, 'The Electrical Resistivity Log as an Aid in Determining some Reservoir Characteristics', *J. Petrol. Technol.* **5**, 1–8.

Cairns, G., Evans, R. L., and Edwards, R. N.: 1996, 'A Time Domain Electromagnetic Survey of the TAG Hydrothermal Mound', *Geophys. Res. Lett.* **23**, 3455–3458.

Chave, A. D., Constable, S. C., and Edwards, R. N..: 1986. 'Electrical Exploration Methods for the Sea Floor', in M.N.. Nabighian (ed.), *Electromagnetic Methods Vol. 2: Applications*, Society of Exploration Geophysicists, Tulsa, OK.

Chave, A. D., and Cox, C. S.: 1982, 'Controlled Electromagnetic Sources for Measuring the Electrical Conductivity Beneath the Oceans', *J. Geophys. Res.* **87**, 5327–5338.

Cheesman, S. J., Edwards, R. N., and Chave, A. D.: 1987, 'On the Theory of Sea Floor Conductivity Mapping using Transient Electromagnetic Systems', *Geophysics* **52**, 204–217.

Cheesman, S. J., Edwards, R. N., and Law, L. K.: 1990, 'A Short Baseline Transient Electromagnetic Method for Use on the Sea Floor', *Geophy. J. Int.* **103**, 431–437.

Cheesman, S. J., Law, L. K., and Edwards, R. N.: 1991, 'Porosity Determinations of Sediments in Knight Inlet Using a Transient Electromagnetic System', *Geomar. Lett.* **11**, 84–89.

Chen, J., Haber, E., and Oldenburg, D. W.: 2002, 'Three-dimensional Numerical Modelling and Inversion of Magnetometric Resistivity Data', *Geophys. J. Int.* **149**, 679–697.

Edwards, R. N.: 1988, 'Two-dimensional Modelling of a Towed Electric Dipole–Dipole EM System: The Optimum Time Delay for Target Resolution', *Geophysics* **53**, 846–853.

Edwards, R. N., Wolfgram, P. A., and Judge, A. S.: 1988, 'The ICE-MOSES Experiment: Mapping Permafrost Zones Electrically Beneath the Beaufort Sea', *Mar. Geophys. Res.* **9**, 265–290.

Edwards, R. N.: 1997, 'On the Resource Evaluation of Marine Gas Hydrate Deposits Using a Sea Floor Transient Electric Dipole–Dipole Method', *Geophysics* **62**, 63–74.

Edwards, R. N., and Chave, A. D.: 1986, 'A Transient Electric Dipole–Dipole Method for Mapping the Conductivity of the Sea Floor', *Geophysics* **51**, 984–987.

Edwards, R. N., Law, L. K., and DeLaurier, J. M.: 1981, 'On Measuring the Electrical Conductivity of the Oceanic Crust by a Modified Magnetometric Resistivity Method', *J. Geophys. Res.* **86**, 11609–11615.

Edwards, R. N., Law, L. K., Wolfgram, P. A., Nobes, D. C., Bone, M. N., Trigg, D. F., and DeLaurier, J. M.: 1985, 'First Results of the MOSES Experiment: Sea Sediment Conductivity and Thickness Determination, Bute Inlet, British Columbia, by Magnetometric Off-shore Electrical Sounding', *Geophysics* **50**, 153–160.

Evans, R. L., Law, L. K., Louis, B., and Cheesman, S. J.: 2000, 'Buried Paleo-Channels on the New Jersey Continental Margin: Channel Porosity Structures from Electromagnetic Surveying', *Mar. Geol.* **170**, 381–394.

Evans, R. L., Sinha, M. C., Constable, S. C., and Unsworth, M. J.: 1994, 'On the Electrical Nature of the Axial Melt Zone at 13 N on the East Pacific Rise', *J. Geophys. Res.* **99**, 77–88.

Evans, R. L., Webb, S. C., Jegen, M., and Sananikone, K.: 1998, 'Hydrothermal Circulation at the Cleft-Vance Overlapping Spreading Center: Results of a Magnetometric Resistivity Survey', *J. Geophys. Res.* **103**, 12321–12338.

Eidesmo, T., Ellinsrud, S., Kong, F-N., Westerdahl, H., and Johansen S.: 2003, 'Method and Apparatus for Determining the Content of Subterranean Reservoirs', *U. S. Patent 6628119 B1*, assigned Den Norske Stats Oljeselskap.

Ellingsrud S., Eidesmo T., Johansen S., Sinha M. C., MacGregor L. M., and Constable S. C.: 2002, 'Remote Sensing of Hydrocarbon Layers by Seabed Imaging (SBL): Results from a cruise offshore Angola', *The Leading Edge* **21**, 972–982.

Ellingsrud S., Eidesmo T., Westerdahl, H. and Kong, F-N.: 2003, 'Method and Apparatus for Determining the Nature of Subterranean Reservoirs', *U. S. Patent 2003/0052685*, assigned Statoil.

Everett, M. E., and Edwards, R. N.: 1993, 'Transient Marine Electromagnetics: The 2–5D Forward Problem', *Geophys. J. Int.* **113**, 545–561.

Hyndman R. D., Yuan T., and Moran, K.: 1999. 'The Concentration of Deep Sea Gas Hydrates from Downhole Electrical Resistivity Logs and Laboratory Data', Earth and Planetary Science Letters, **172**, 167–177.

McBarnet, A.: 2004, 'All at Sea with EM', *Offshore Eng.* **29**, 20–22.

Nobes, D. C., Law, L. K., and Edwards, R. N.: 1986, 'The Determination of Resistivity and Porosity of the Sediment and Fractured Basalt Layers near the Juan de Fuca ridge', *Geophys. J. R. Astronom. Soc.* **86**, 289–318.

Schwalenberg, K., Willoughby, E., Mir, R., and Edwards, R. N.: 2005, 'Marine Gas Hydrate Electromagnetic Signatures in Cascadia and their Correlation with Seismic Blank Zones', *First Break* **23**, 57–63.

Sinha, M. C., Navin, D. A., MacGregor, L. M., Constable, S. C., Peirce, C., White, A., Heinson, G., and Inglis, M. A.: 1997, 'Evidence for Accumulated Belt Beneath the Slow-spreading Mid-Atlantic Ridge', *Phil. Trans. R. Soc. Lond. A* **355**, 233–253.

Srnka L., 2003, 'Remote Reservoir Resistivity Mapping', *U. S. Patent 6603313*, assigned Exxon-Mobil.

Unsworth, M. J., Travis, B. J., and Chave, A. D.: 1993, 'Electromagnetic Induction by a Finite Electric Dipole Source over a 2-D Earth', *Geophysics* **58**, 198–214.

Webb, S. C., Constable, S. C., Cox, C. S., and Deaton, T. K.: 1985, 'A Sea Floor Electric Field Instrument', *J. Geoelec. Geomag.* **37**, 1115–1130.

Webb, S. C., and Edwards, R. N.: 1995, 'On the Correlation of Electrical Conductivity and Heat Flow in Middle Valley, Juan de Fuca Ridge', *J. Geophys. Res.* **100**(22), 523–22,532.

Yu, L., and Edwards, R. N.: 1991, 'The Detection of Lateral Anisotropy of the Ocean Floor by Electromagnetic Methods', *Geophys. J. Int.* **108**, 433–441.

Yu, L., Evans, R. L., and Edwards, R. N.: 1997, 'Transient Electromagnetic Responses in Seafloor with Tri-axial Anisotropy', *Geophys. J. Int.* **129**, 300–306.

Yuan, J., and Edwards, R. N.: 2000, 'The Assessment of Marine Gas Hydrate through Electrical Remote Sounding: Hydrate Without a BSR?', *Geophys. Res. Lett.* **27**, 2397–2400.

Ziolkowski A., and Hobbs B.A.: 2003, 'Detection of Subsurface Resistivity Contrasts with Application to Location of Fluids', *International Patent WO 03/023452 A1*, assigned Edinburgh University.